

Dear Dr. van den Broeke,

Thank you for the thorough editing of our manuscript. We applied all of your suggestions.

Besides word-level changes, we rephrased (p.6 l. 226-227): “We do not consider that the uncertainty applying on an estimated FAC10 can be smaller than the one of FAC10 observations.” to “We set 0.3 m, the uncertainty related to FAC measurements (Section 2.2), as the minimum possible uncertainty on any empirically estimated FAC10.”

Also, regarding your comment (p. 19, l.414): “Here you could mention that the 2012 melt event must somehow have caused a FEC decrease in the DSA.”: Although it is true at the conceptual level, the magnitude of the potential FAC decrease in the DSA is much lower than the spatial heterogeneity applying on FAC measurements. We therefore would like to avoid making hypothesis on a FAC change below our detection limit.

Thanks again for your help.

Best regards,

Baptiste Vandecrux on behalf of the co-authors

1 **Firn data compilation reveals widespread decrease of firn air content** 2 **in West Greenland**

3 Baptiste Vandecrux^{1,2}, Michael MacFerrin³, Horst Machguth^{4,5}, William T. Colgan¹, Dirk van As¹,
4 Achim Heilig⁶, C. Max Stevens⁷, Charalampos Charalampidis⁸, Robert S. Fausto¹, Elizabeth M.
5 Morris⁹, Ellen Mosley-Thompson¹⁰, Lora Koenig¹¹, Lynn N. Montgomery¹¹, Clément Miège¹²,
6 Sebastian B. Simonsen¹³, Thomas Ingeman-Nielsen², Jason E. Box¹

7
8 ¹ Department of Glaciology and Climate, Geological Survey of Denmark and Greenland, Copenhagen, Denmark.

9 ² Department of Civil Engineering, Technical University of Denmark, Lyngby, Denmark.

10 ³ Cooperative Institute for Research in Environmental Sciences, University of Colorado, Boulder, CO USA

11 ⁴ Department of Geosciences, University of Fribourg, Fribourg, Switzerland

12 ⁵ Department of Geography, University of Zurich, Zurich, Switzerland

13 ⁶ Department of Earth and Environmental Sciences, LMU, Munich, Germany

14 ⁷ Department of Earth and Space Sciences, University of Washington, WA USA

15 ⁸ Bavarian Academy of Sciences and Humanities, Munich, Germany

16 ⁹ Scott Polar Research Institute, Cambridge University, United Kingdom

17 ¹⁰ Byrd Polar and Climate Research Center and Department of Geography, Ohio State University, Columbus, OH USA.

18 ¹¹ National Snow and Ice Data Center, University of Colorado, Boulder, CO, United States

19 ¹² Department of Geography, Rutgers University, Piscataway, NJ, United States

20 ¹³ DTU Space, National Space Institute, Department of Geodynamics, Technical University of Denmark, Kgs. Lyngby,
21 Denmark

22
23 *Correspondence to:* B. Vandecrux (bava@byg.dtu.dk)

24
25 **Abstract.** A ~~thick and~~ porous layer of multiyear snow known as firn covers the Greenland ice-sheet interior. The firn layer
26 buffers the ice-sheet contribution to sea-level rise by retaining a fraction of summer melt as liquid water and refrozen ice. In
27 this study we quantify the Greenland ice-sheet firn air content (FAC), an indicator of meltwater retention capacity,
28 ~~associated with~~based on 360 point observations. We quantify FAC in both the uppermost 10 m and the entire firn column
29 before interpolating FAC over the entire ice-sheet firn area as an empirical function of long-term mean air temperature (\overline{T}_a)
30 and net snow accumulation (\overline{c}). We ~~assess-estimate~~ a total ice-sheet wide FAC of $26\,800 \pm 1\,840 \text{ km}^3$, of which $6\,500 \pm 450$
31 km^3 resides within the uppermost 10 m of firn, during-for the 2010-2017 period. In the dry snow area ($\overline{T}_a \leq -19^\circ\text{C}$), FAC has
32 not changed significantly since 1953. In the low accumulation percolation area ($\overline{T}_a > -19^\circ\text{C}$ and $\overline{c} \leq 600 \text{ mm w.eq. yr}^{-1}$), FAC
33 has decreased by $23 \pm 16\%$ between 1998-2008 and 2010-2017. This reflects a loss of firn retention capacity of between 150
34 $\pm 100 \text{ Gt}$ and $540 \pm 440 \text{ Gt}$ respectively from the top 10 m and entire firn column. The top 10 m FACs simulated by three
35 regional climate models (HIRHAM5, RACMO2.3p2, and MARv3.9) agree within 12% with observations. However, model
36 biases in the total FAC and marked regional differences highlight the need for caution when using models to quantify the
37 current and future FAC and firn retention capacity.

38 1. Introduction

39 As a consequence of the atmospheric and oceanic warming associated with anthropogenic climate change, the Greenland ice
40 sheet ([GrIS](#)) is losing mass at an accelerating rate. The ~~ice-sheet~~[GrIS](#) is now responsible for approximately 20% of
41 contemporary sea-level rise (Bindoff et al., 2013; Nerem et al. 2018). Over half this ~~ice-sheet~~[GrIS](#) mass loss stems from
42 summer surface melt and subsequent meltwater runoff into the ocean (van den Broeke et al., 2016). While most meltwater
43 runoff originates from the low-elevation ablation area, the surface melt area is now expanding into the high-elevation firm-
44 covered interior of the ~~Greenland ice-sheet~~[GrIS](#) (Mote et al. 2007; Nghiem et al., 2012). Rather than flowing horizontally,
45 most of the meltwater produced at the surface of the firm area percolates vertically into the underlying firm where it refreezes,
46 and thereby does not contribute to sea-level rise (Harper et al., 2012). Hence, the meltwater retention capacity of Greenland's
47 firm is a non-trivial parameter in the sea-level budget.

48
49 Assessing meltwater retention capacity of the firm in Greenland requires knowledge of both the extent of the firm area, as
50 well as the spatial distribution of depth-integrated firm porosity or firm air content (FAC). The extent of the firm area can be
51 tracked using the firm line, which Benson (1962) described as “the highest elevation to which the annual snow cover recedes
52 during the melt season”. Recently, Fausto et al. (2018a) updated the methods from Fausto et al. (2007) and presented maps
53 of remotely sensed end-of-summer snowlines over the 2000-2017 period. These maps effectively provide an annual
54 delineation of Greenland's firm area. FAC is the integrated volume of air contained within the firm from the surface to a
55 certain depth per unit area (van Angelen et al., 2013; Ligtenberg et al., 2018). FAC quantifies the maximum pore volume
56 available per unit area to retain percolating meltwater, either in liquid or refrozen form (Harper et al., 2012; van Angelen et
57 al. 2013). Previously, ice-sheet-wide firm retention capacity has been estimated using simplifying assumptions (Pfeffer et al.,
58 1991) or unconstrained regional climate model (RCM) simulations (van Angelen et al., 2013). Harper et al. (2012) provided
59 a first empirical estimate of the firm's meltwater retention capacity in the ~~ice-sheet~~[GrIS](#) percolation area using two years of
60 observations (2007 and 2008) at 15 sites in western Greenland. While pioneering, their approach did not acknowledge the ~~ice~~
61 ~~sheet~~[GrIS](#)'s diverse firm regimes (Forster et al. 2014; Machguth et al., 2016). Ligtenberg et al. (2018) provided an RCM
62 simulation of FAC that generally compares well against observations in 62 firm cores, but substantially underestimated FAC
63 in the western percolation area.

64
65 The depth to which meltwater may percolate, and therefore the depth range over which FAC must be integrated to constrain
66 meltwater retention capacity, varies with melt intensity and firm permeability (Pfeffer et al., 1991). This makes the maximum
67 depth of meltwater percolation both temporally and spatially variable, as highlighted by the following studies. Braithwaite et
68 al. (1994) and Heilig et al. (2018) reported meltwater refreezing within the top 4 m of firm in western Greenland respectively
69 at ~1500 m a.s.l. during summer 1991 and at 2120 m a.s.l. during the 2016 melt season. Both studies indicate that, at specific
70 sites and years, meltwater is stored in near-surface ~~FAC~~[firm](#). However, firm temperature measurements in 2007-2009 at 1555

71 m a.s.l. in west Greenland (Humphrey et al., 2012) as well as the presence of firn aquifer at depth greater than 10 m in
 72 southeast Greenland (Miège et al., 2016) both show that meltwater can percolate below 10 m depth in the firn. This deep
 73 percolation implies that, for certain firn conditions and given sufficient meltwater, the FAC of the total firn column, from the
 74 surface to the firn-ice transition, may be used for meltwater retention. Finally, Machguth et al. (2016) show that percolation
 75 depth may not increase linearly with meltwater production, and instead low-permeability ice layers can limit even abundant
 76 meltwater from percolating into the entire firn column. Given the complexity of meltwater percolation and the paucity of
 77 percolation observations, reasonable upper and lower bounds of the meltwater retention capacity of firn can be estimated by
 78 determining FAC through the total firn column (FAC_{tot}) and within the uppermost 10 m of firn column (FAC_{10}), respectively
 79 (Harper et al. 2012). FAC_{tot} is also valuable information to convert remotely sensed surface height changes into mass
 80 changes (Sørensen et al., 2011; Simonsen et al. 2013; Kuipers Munneke et al. 2015a).

81
 82 In this study, we first compile a dataset of 360 firn observations density profiles, collected between 1953 and 2017, and
 83 quantify the observed FAC. We then extrapolate these point-scale observations across the entire ice sheet GrIS firn area as
 84 empirical functions of long-term mean air temperature and mean snow accumulation. The point observations are thereby
 85 used to resolve the spatial distribution of FAC, but also, where possible, its temporal evolution. We use a simple
 86 extrapolation to estimate FAC_{tot} from FAC_{10} where firn cores do not extend to the firn-ice transition. Spatial integration of
 87 FAC_{10} and FAC_{tot} over the firn area permits estimating lower and upper bounds, respectively, of the Greenland-GrIS firn's
 88 meltwater retention capacity. Finally, we evaluate the FAC simulated by three RCMs, that are commonly used to evaluate
 89 ice-sheet-wide firn meltwater retention capacity, but that have never been compared to such an extensive firn dataset.

90 2. Data and methods

91 2.1. Firn core dataset and firn area delineation

92 We compiled 340 previously published Greenland ice sheet GrIS firn-density profiles of at least 5 m in depth (Table 1). To
 93 these, we added an additional 20 cores extracted in 2016 and 2017, for which firn density was measured at 10 cm resolution
 94 following the same procedure as Machguth et al. (2016). When near-surface snow densities were missing, we assigned a
 95 density of 315 kg m^{-3} (Fausto et al., 2018b) to the top centimetre and interpolated over the remaining gaps in density profiles
 96 using a logarithmic function of depth fitted to the available densities.

97
 98 **Table 1. List of the publications presenting the firn cores used in this study.**

Source	Number of cores	Source	Number of cores
Albert and Shultz (2002)	1	Langway (1967)	1
Alley (1987)	1	Lomonaco et al. (2011)	1

Bader (1954)	1
Baker (2012)	1
Benson (1962)	55
Bolzan and Strobel (1999)	9
Buchardt et al. (2012)	8
Clausen et al. (1988)	8
Colgan et al. (2018)	1
Fischer et al. (1995)	14
Forster et al. (2014)	5
Hawley et al. (2014)	8
Harper et al. (2012)	32
Jezeq (2012)	1
Kameda et al. (1995)	1
Koenig et al. (2014)	3
Kovacs et al. (1969)	1

Machguth et al. (2016)	28
Mayewski and Whitlow (2016a)	1
Mayewski and Whitlow (2016b)	1
Miège et al. (2013)	3
Morris and Wingham (2014)	66
Mosley-Thompson et al. (2001)	47
Porter and Mosley-Thompson (2014)	1
Reed (1966)	1
Renaud (1959)	7
Spencer et al. (2001)	8
Steen-Larsen et al. (2011)	1
Vallelonga et al. (2014)	1
van der Veen et al. (2001)	10
Wilhelms (1996)	13
This study	20

99

100 We use the end-of-summer snowlines from Fausto et al. (2018a) to delineate the minimum firm area detected during the
101 2000-2017 period. This 1 405 500 km² area, where snow is always detected during the 2000-2017 period, is taken to
102 represent the ~~ice-sheet~~GrIS's current firm area. Moving this firm line 1 km inward or outward, the resolution of the product
103 from Fausto et al. (2018a), suggests an uncertainty of ±17 250 km² (~1%). Additional uncertainty applies ~~to~~ the margin of
104 the firm area where ~~ephemeral-transient~~ firm patches may exist outside of our delineation. Owing to the inherent thinness of
105 firm at the lower elevation boundary of the firm area, we expect these omitted firm patches to play a negligible role in the
106 overall meltwater retention capacity of the firm area.

107 2.2. Calculation of FAC₁₀

108 For a discrete density profile composed of N sections and reaching a depth z, the FAC in meters is calculated as:

$$109 \quad FAC_z = \sum_{k=1}^N m_k \left(\frac{1}{\rho_k} - \frac{1}{\rho_{ice}} \right) \quad [1]$$

110 where, for each depth interval k, ρ_k is the firm density and m_k is the firm mass. ρ_{ice} is the density of the ice, assumed to be
111 917 kg/m³.

112
113 With 121 cores shorter than 10 m in our dataset, we extrapolate shallow measurements to a depth of 10 m. We do this by
114 finding the longer than 10 m core that best matches the FAC-versus-depth profile of the shorter than 10 m core, with the
115 lowest root mean squared difference (RMSD) amongst all available cores. We then append the bottom section of this longer

116 than 10 m core to the FAC profile of the shorter than 10 m core (see Figure S1 of the Supplementary Material). When testing
117 this methodology on the available 10 m long cores, from which we remove the deepest 3 m of the FAC profile, we find a
118 mean difference between extrapolated and real $FAC_{10} < 1\%$ and an RMSD of 0.15 m.

119
120 We assess the accuracy of the firn density measurements, as well as the effect of spatial heterogeneity, by comparing FAC_{10}
121 measurements located within 1 km and collected in the same year (Figure S2 of the Supplementary Material). A standard
122 deviation below 0.15 m is found in the majority of the co-located and contemporaneous FAC_{10} observations (20 of 27 groups
123 of comparable observations). We correspondingly assign an uncertainty of ± 0.3 m, twice this standard deviation, to FAC_{10}
124 measurements.

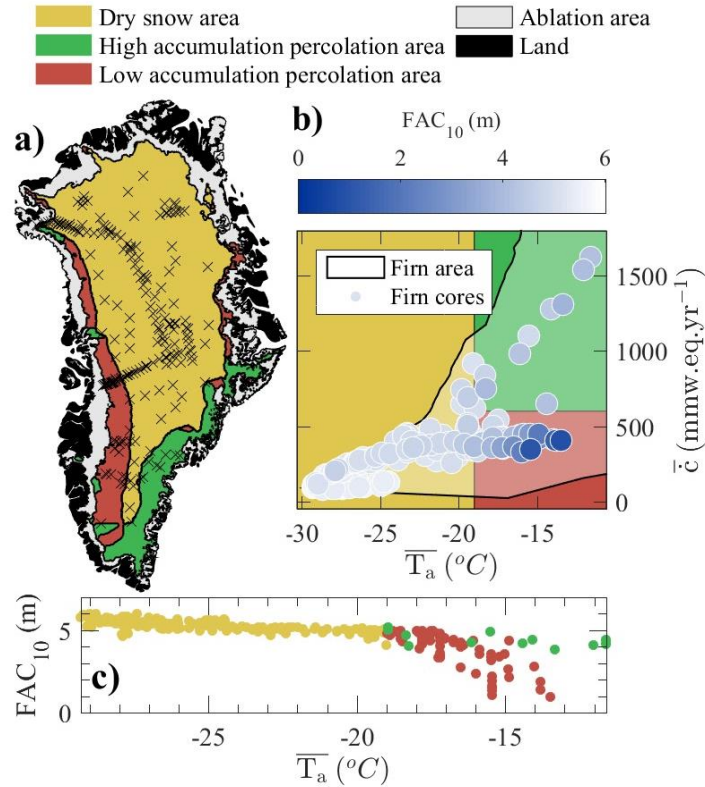
125 **2.3. Zonation of firn air content**

126 The FAC_{10} is calculated from firn density, which depends, among other parameters, on the local near-surface air temperature
127 and snowfall rate (Shumskii, 1964). Air temperature is a proxy for summer melt and subsequent refreezing within the firn, as
128 well as firn temperature and compaction rates. Through these processes, increasing air temperature acts to decrease FAC
129 (Kuipers Munneke et al., 2015b). On the other hand, snow accumulation introduces low-density fresh snow at the surface.
130 Increasing snowfall thus acts to increase FAC. To put our FAC_{10} measurements in their climatic context, we extract the long-
131 term (1979-2014) average annual net snow accumulation \bar{c} (snowfall – sublimation) and air temperature \bar{T}_a for each FAC_{10}
132 measurement location from the nearest 5 km² cell of the Modèle Atmosphérique Régional (MARv3.5.2; Fettweis et al.,
133 2017).

134
135 Following the terminology of Benson (1962), we define three regions where FAC_{10} shows distinct regimes: (1) the dry snow
136 area (DSA, yellow area in Figure 1a); (2) the low accumulation percolation area (LAPA, red area in Figure 1a); (3) the high
137 accumulation percolation area (HAPA, green area in Figure 1a). The DSA encompasses low temperature regions of high
138 altitude and/or latitude where melt is uncommon and where FAC_{10} can be related by a linear function of \bar{T}_a (yellow markers
139 in Figure 1c). Two distinct firn regimes emerge towards higher \bar{T}_a , meaning lower altitude and/or latitude. Firstly, towards
140 lower \bar{c} , in the LAPA, more scatter appears in FAC_{10} and the slope of the FAC_{10} temperature dependency changes. Secondly,
141 towards higher \bar{c} , in the HAPA, the few available FAC_{10} observations describe a similar temperature dependency as in the
142 DSA, even though they are in relatively warm regions where melt occurs. FAC_{10} observations in the HAPA are up to five
143 times higher than at locations with similar \bar{T}_a in the LAPA (Figure 1c).

144
145 The boundary that delineates the cold (DSA) and warm regions (LAPA and HAPA) can be defined as the temperature where
146 an inflection occurs in the linear dependency of FAC_{10} on \bar{T}_a (Figure 1c). We interpret the slope break in the temperature
147 dependence of FAC_{10} as the upper limit of frequent meltwater percolation and refreezing within the firn which Benson et al.

148 (1962) defined as the dry snow line. While the transition between cold and warm areas is gradual in practice, for our analysis
 149 we set this boundary to $\bar{T}_a = -19^\circ\text{C}$. Our LAPA and HAPA here stretch from the dry snow line to the firm line and therefore
 150 also include the so-called wet snow facies defined by Benson et al. (1962). The snowfall boundary that delineates the low
 151 and high accumulation percolation areas is more difficult to characterize. There are insufficient firm observations available
 152 along the transition from LAPA to HAPA. The snowfall boundary could be anywhere between 543 mm w.eq. yr⁻¹ (the
 153 highest accumulation LAPA core, Figure 1b) and 647 mm w.eq. yr⁻¹ (the lowest accumulation HAPA core, Figure 1b).
 154 Acknowledging this uncertainty, we chose the round value of $\bar{c} = 600$ mm w.eq. yr⁻¹ to separate LAPA and HAPA. The
 155 spatial delineations of the DSA, LAPA and HAPA are illustrated in Figure 1a.



156
 157 **Figure 1. a) Spatial distribution of the FAC₁₀ dataset. The DSA, HAPA and LAPA are indicated respectively using yellow, green**
 158 **and red areas. b) Distribution of the dataset in the accumulation-temperature space (\bar{c} and \bar{T}_a). FAC₁₀ value is indicated by a**
 159 **coloured marker. Black lines and shaded areas indicate the extent of firm in the accumulation-temperature space. c) Temperature**
 160 **dependency of FAC₁₀ in the DSA (yellow markers), LAPA (red markers) and HAPA (green markers).**

161 2.4. FAC₁₀ interpolation

162 | To interpolate point-scale observations of FAC₁₀ over the entire [ice-sheetGrIS](#) firm area, we describe FAC₁₀ observations
 163 using empirical functions of long-term mean air temperature and net snowfall. The derivation of these empirical functions is

164 described in the following sections and an overview of their general form as well as the data used to constrain them are
 165 presented in Table 2.

166

167 **Table 2. Overview of the empirical functions fitted to FAC_{10} observations in each region of the firm area.**

Area	Period	Form	Observations used for fitting
DSA & upper HAPA	1953 - 2017	Linear function of \bar{T}_a (Eq. 2)	259 from the DSA 19 from the HAPA
LAPA & HAPA	2010 - 2017	<ul style="list-style-type: none"> Smoothed bilinear function of \bar{T}_a and \bar{c}. 	25 from the LAPA 10 from the HAPA 6 selected from firm line in the HAPA
LAPA	1998 - 2008	<ul style="list-style-type: none"> Cannot exceed the FAC_{10} estimated with Eq. 2. 	38 from the LAPA 1 from the HAPA 6 selected from the firm line in the HAPA

168

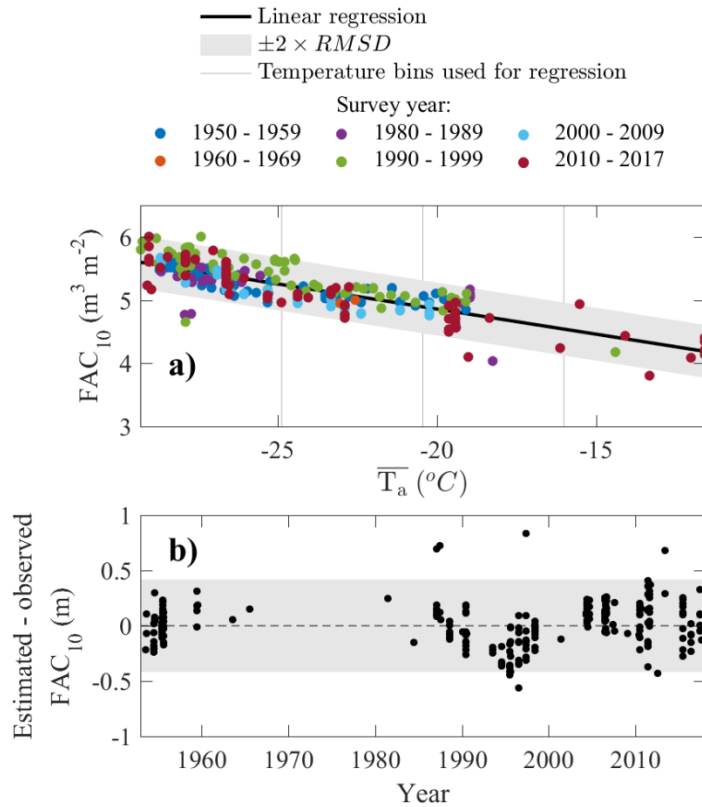
169 2.4.1. Dry snow area

170 In the DSA, the 259 FAC_{10} observations obtained between 1953 and 2017 can be approximated by a linear function of their
 171 local \bar{T}_a (Figure 1c). This dependency is the same for the 19 FAC_{10} observations from the upper HAPA available between
 172 1981 and 2014. We consequently include these observations so that the linear relationship remains valid in the upper HAPA
 173 (Section 2.4.2). These 278 FAC_{10} observations are then binned into four equal \bar{T}_a ranges to avoid the overrepresentation of
 174 clustered data (Figure 2a). Eventually, a linear function of \bar{T}_a is fitted to the bins' average FAC_{10} using least squares
 175 method to estimate the FAC_{10} in the DSA:

$$176 \quad FAC_{10}(\bar{T}_a) = -0.08 * \bar{T}_a + 3.27 \quad [2]$$

177 We assign to any FAC_{10} estimated in the DSA using Eq. 2 an uncertainty equal to twice the regression's RMSD: 0.4 m.
 178 Although FAC_{10} is also dependant on \bar{c} , the residuals from Eq. 2 do not present any correlation with their respective \bar{c}
 179 values. It indicates that because of the intrinsic co-variability of \bar{c} and \bar{T}_a , most of the variations in observed FAC_{10} can
 180 be explained using either \bar{c} or \bar{T}_a . Insufficient data are available to ~~disambiguate-separate~~ the role of \bar{c} and \bar{T}_a in FAC_{10}
 181 variations in the DSA. We therefore choose to use only \bar{T}_a in Eq. 2.

182



183

184 **Figure 2. a) Linear function of \overline{T}_a fitted to FAC₁₀ observations from the DSA and upper HAPA. b) Residual between estimated**
 185 **(using linear regression) and observed FAC₁₀ as a function of survey year.**

186

187

2.4.2. Percolation areas

188

In the LAPA and in the HAPA, FAC₁₀ observations exhibit a more complex dependency on \bar{c} and \overline{T}_a (Figure 1b and 1c). Additionally, observations are unevenly distributed in space and time. Thus to reveal the temporal trends in FAC₁₀, the observation dataset is divided into two time slices that each contain enough FAC₁₀ observations to describe the spatial pattern of FAC₁₀ and constrain our empirical functions.

192

193

Over the 2010-2017 period, 25 FAC₁₀ observations were made in the LAPA, stretching from the upper boundary of the LAPA down to the vicinity of the firn line. During that same period, 10 firn cores were collected in the HAPA. Unfortunately, in addition to their small number, the cores are located relatively far into the interior of the ice sheet and do not describe how the FAC₁₀ decreases in parts of the HAPA closer to the firn line. We consequently complement these firn cores with 6 sites, selected on the remotely sensed firn line, where FAC₁₀ is assumed to be null (Figure S3). FAC₁₀ in the LAPA and HAPA during 2010-2017 is then described by a smoothed bilinear function of \overline{T}_a and \bar{c} fitted through least

198

199 squares method to the available observations (Figure 3a). We do not allow that function to exceed the linear function of \bar{T}_a
200 that describes FAC_{10} measurements in the DSA and in the upper HAPA (Eq. 2) or to predict FAC_{10} below 0 m.

201

202 Prior to 2010, insufficient data are available to document the FAC_{10} in the HAPA. In the LAPA, however, 35 observations
203 were made between 2006 and 2008 and three cores were collected in 1998. These measurements are used to describe the
204 FAC_{10} in LAPA during the 1998-2008 period by a smoothed bilinear function of \bar{T}_a and \bar{c} . To ensure that our empirical
205 function has realistic values towards the transition with the HAPA, we also include one core collected in the HAPA in 1998.
206 We also include the previously described six locations from the firm line (Figure 3a). Although observation locations in
207 1998-2008 and 2010-2017 can be different, few samples available at the same sites (e.g. Crawford Point, Dye-2) in both time
208 slices ~~ensure-comfirm~~ that FAC_{10} changes are more likely due to a temporal evolution rather than from the different spatial
209 coverage of each period's constraining dataset.

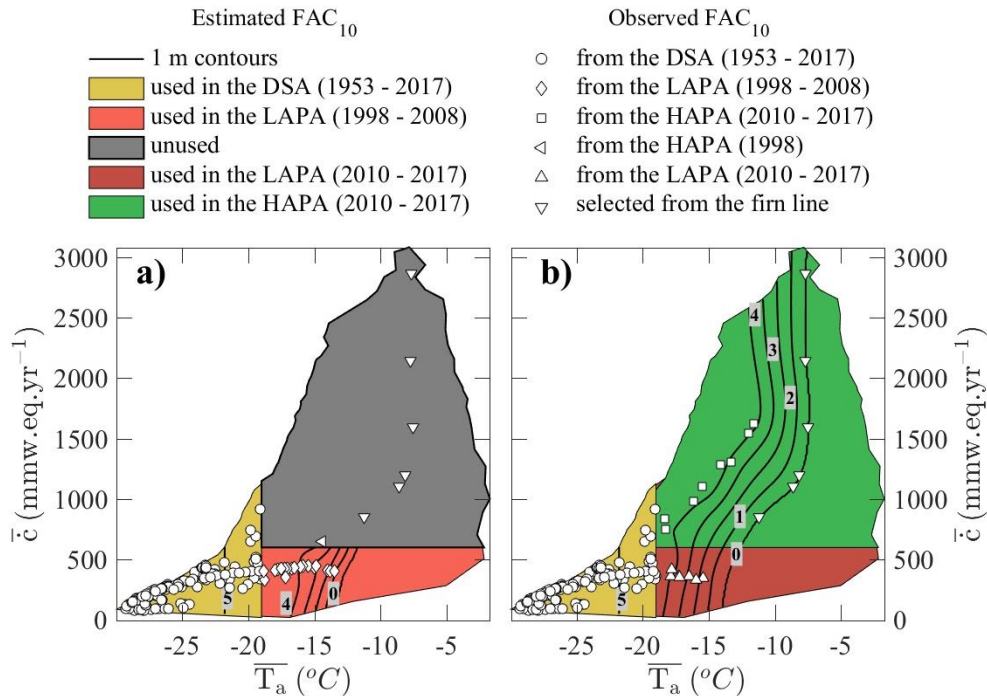
210

211 The empirical functions used to estimate the FAC_{10} in the LAPA and HAPA (Figure 3), when compared to FAC_{10}
212 observations, have a RMSD of 0.28 m in the LAPA over the 1998-2008 period, 0.27 m in the LAPA over the 2010-2017
213 period and 0.17 m in the HAPA over the 2010-2017 period.

214

215 We investigate the robustness of our empirical functions in the HAPA and LAPA using, for each period separately, the
216 following sensitivity analysis. For 1000 repetitions, we apply four types of perturbations to the FAC_{10} observations and then
217 re-fit our empirical functions. The effect of the availability of measurements in the LAPA is tested by randomly excluding
218 four observations in that region (16% and 11% of observations in 2010-2017 and 1998-2008, respectively). The effect of
219 uncertainty in the firm line location in the (\bar{T}_a, \bar{c}) space is tested by adding a normally distributed noise with mean zero and
220 standard deviation 3°C to the \bar{T}_a of firm-line-derived FAC_{10} (illustrated in Figure S3). The effect of the uncertain FAC_{10}
221 value at the firm line is assessed by assigning to firm-line-derived points a random FAC_{10} value between 0 and 1 m. Finally,
222 the effect of the smoothing applied to the bilinear interpolation of FAC_{10} measurements is assessed by modifying the amount
223 of smoothing applied. Following 1000 repetitions of the above-mentioned four perturbations to the FAC_{10} observations, we
224 then calculate the standard deviation of all empirically estimated FAC_{10} values within the (\bar{T}_a, \bar{c}) parameter space. We then
225 double this standard deviation to approximate the 95% uncertainty envelope for empirically estimated FAC_{10} in the LAPA
226 and HAPA. ~~We do not consider that the uncertainty applying on an estimated FAC_{10} can be smaller than the one of FAC_{10}
227 observations.~~ We ~~consequently~~ set 0.3 m, the uncertainty related to FAC measurements (Section 2.2), as the minimum
228 possible uncertainty on any empirically estimated FAC_{10} .

229



230

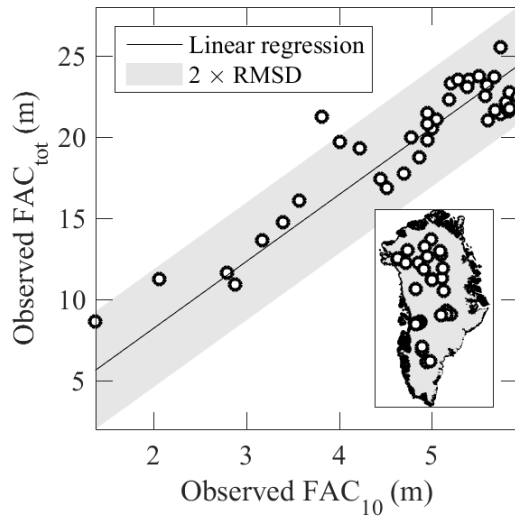
231 **Figure 3. Contours (labelled black lines) of the empirical functions of \bar{T}_a and \bar{c} used to estimate FAC_{10} along with the FAC_{10}**
 232 **observations used to constrain the functions. Two functions could be constructed: (a) describing FAC_{10} in the LAPA during 1998-**
 233 **2008 and (b) describing FAC_{10} in the LAPA and HAPA during 2010-2017.**

234 **2.5. Estimation of FAC_{tot}**

235 FAC_{tot} should be integrated from the ice-sheet surface down to the depth where firn reaches the density of ice (Ligtenberg et
 236 al., 2018). This depth varies in space and time across the [ice-sheetGrIS](#) but is poorly documented. Additionally, the RCM
 237 HIRHAM5 (evaluated in Section 3.3) does not reach ice density at the bottom of its column in certain locations. We
 238 therefore calculate FAC_{tot} as the vertically integrate FAC from the surface to a standard 100 m depth. Only 29 of our 360 firn
 239 observations reach depths greater than 100 m. We therefore complement these core observations with 13 ground-penetrating
 240 radar observations of FAC_{tot} from Harper et al. (2012). Using the least squares method with an intercept of zero, we fit the
 241 following linear regression between FAC_{10} and FAC_{tot} (Figure 4):

242
$$FAC_{tot} = 4.1 * FAC_{10} \quad [3]$$

243 This function infers that FAC_{tot} is approximately 410% of FAC_{10} . While we acknowledge this relation is straightforward, we
 244 highlight that it is statistically robust. We assign 3.6 m, twice the RMSD of the linear regression, as the typical uncertainty
 245 [applying on for](#) an estimated FAC_{tot} value that can in theory vary between 0 and ~25 m.



246

247 **Figure 4. Linear regression used to estimate FAC_{tot} from FAC_{10} .**

248 As a result of deriving FAC_{tot} as a function of FAC_{10} (Eq. 3), any change in FAC_{10} between two dates implies a proportional
 249 change in FAC_{tot} over the same time period. This co-variation neglects that near-surface changes in the firm slowly propagate
 250 to greater depth with thermal conduction and downward mass advection (Kuipers Munneke et al., 2015b). We therefore note
 251 that for a decreasing FAC_{10} (see Section 3.2.1), our estimated change in FAC_{tot} corresponds to the maximum possible change
 252 associated with the whole firm column having sufficient time to adapt to the new surface conditions.

253 2.6. Spatially integrated FAC and retention capacity

254 We define, for any ice-sheet region, the spatially integrated FAC as the cumulated volume of air within that region either in
 255 the top 10 m of firm or for the total firm column (top 100 m). The uncertainty associated with the empirically estimated
 256 FAC_{10} and FAC_{tot} at a given location are not independent from other locations because the same functions of \bar{T}_a and \bar{c} are
 257 applied across the [ice sheet GrIS](#). Consequently, we consider that the uncertainty of the mean FAC in a specific region is the
 258 mean of FAC uncertainty values therein and that the uncertainty of spatially integrated FAC is the sum of the uncertainty
 259 values in the considered region.

260

261 We use the estimated FAC to calculate the meltwater retention capacity of the firm. Harper et al. (2012) defined the firm
 262 retention capacity as the amount of water that needs to be added to the firm to bring its density to 843 kg m^{-3} , the density of
 263 firm saturated by refrozen meltwater measured in firm cores.

264 2.7. Comparison with Regional Climate Models

265 We compare our FAC_{10} observations and spatially integrated FAC estimates to the firm products available from three RCMs:
266 HIRHAM5, RACMO2.3p2 and MARv3.9. HIRHAM5 output is available at 5.5 km spatial resolution and is presented in
267 Langen et al. (2017). Two versions of HIRHAM5 are used: with linear parametrization of surface albedo (thereafter referred
268 as HH_LIN) and MODIS-derived albedo (thereafter referred as HH_MOD). RACMO2.3p2, presented by Noël et al. (2018),
269 provides FAC at a 5.5 km resolution. MARv3.9 is presented in Fettweis et al. (2017), only simulates FAC_{10} because of its
270 shallow subsurface domain and has a spatial resolution of 15 km.

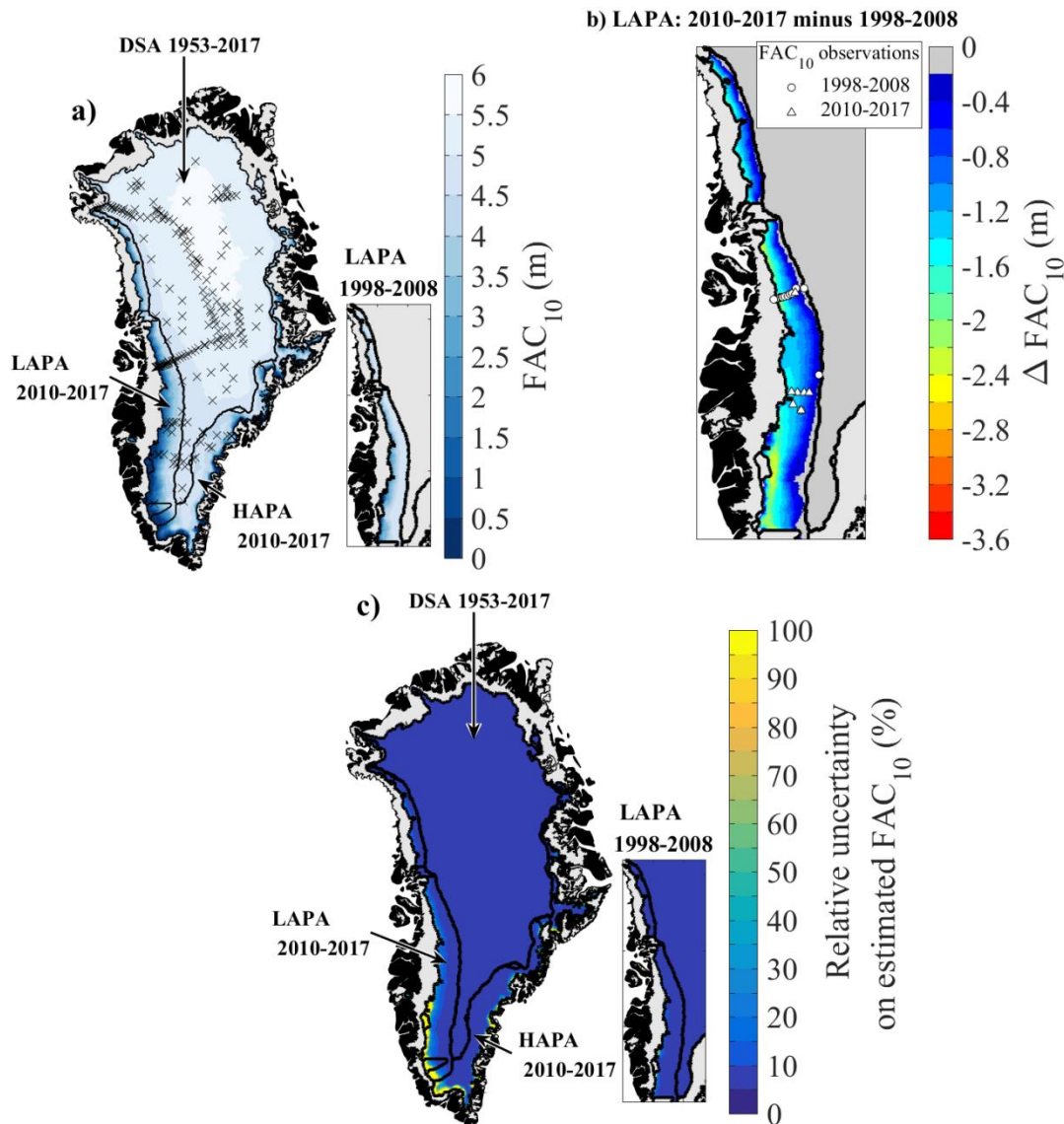
271 3. Results and discussion

272 3.1. Spatio-temporal distribution of FAC

273 In the DSA, we consider the absence of a temporal trend in the deviation between measured FAC_{10} and FAC_{10} estimated
274 using the linear function of \bar{T}_a (Figure 2b) as evidence of unchanging FAC_{10} in that area between 1953 and 2017. This
275 inference of widespread stable FAC in the DSA is confirmed at point scale by firn cores in our dataset taken at the same sites
276 but decades apart, showing the same FAC (Summit, Camp Century, e.g.). This result is also corroborated by recent firn
277 modelling at weather stations located in the DSA (Vandecrux et al. 2018).

278
279 Using the 5x5 km \bar{T}_a and \bar{c} grids from Fettweis et al. (2017) and the empirical functions presented in Figure 3, we map the
280 FAC_{10} and its uncertainty across the GrIS firm area ~~of the ice sheet~~ (Figure 5). From these maps we calculate an average
281 FAC_{10} of 5.2 ± 0.3 m in the DSA over the 1953-2017 period and of 3.0 ± 0.4 m in the HAPA during the 2010-2017 period.
282 Within the LAPA, we calculate an average FAC_{10} of 3.9 ± 0.3 m during the 1998-2008 period, which decreases by 23 % to
283 3.0 ± 0.3 m by-in the 2010-2017 period. Spatially, the FAC_{10} loss in the LAPA is concentrated in a 60 km wide band above
284 the firn line in western Greenland (Figure 5b).

285
286



288 **Figure 5. a) FAC₁₀ maps and location of the FAC₁₀ measurements. b) Change in FAC₁₀ between 1998-2008 and 2010-2017 in the**
 289 **LAPA. c) Maps of the relative uncertainty of the FAC₁₀ map.**
 290

291
 292 We find that during the 2010-2017 period, the entire firn area contained $6\,500 \pm 450 \text{ km}^3$ of air ~~content~~ within the top 10 m
 293 and ~~potentially~~ up to $26\,800 \pm 1\,840 \text{ km}^3$ within the whole firn column (Table 3). About $83 \pm 5\%$ of this air content is
 294 ~~contained~~ found in the DSA, which represents 74% of the firn area. The HAPA, covering 12% of the firn area, contains $8 \pm$
 295 1% of ~~ice sheet wide firn air content~~ GrIS FAC, both for the top 10 m and the whole firn column.

297 **Table 3. Spatially integrated FAC and firn retention capacity over each ice sheet region.**

Area	Period	Spatially integrated FAC (km ³)			Firn storage capacity (Gt)		
		Upper 10 m		Total firn column	Upper 10 m		Total firn column
DSA	1953 – 2017	5 400 ± 310	22 300 ± 1 280	4 200 ± 290	12 800 ± 1 170		
LAPA	1998 – 2008	750 ± 60	3 100 ± 240	550 ± 50	1 490 ± 220		
LAPA	2010 – 2017	580 ± 60	2 400 ± 250	400 ± 50	950 ± 220		
HAPA	2010 – 2017	530 ± 80	2 200 ± 320	370 ± 70	960 ± 290		
All	2010 – 2017	6 500 ± 450	26 800 ± 1 840	5 000 ± 410	14 700 ± 1 600		

298

299 The LAPA, which comprises 14% of the firn area, contained $9 \pm 1\%$ of ice-sheet-wide firn air content in the period 2010-
300 2017. Decreasing FAC₁₀ between 1998-2008 and 2010-2017 yields a loss of $170 \pm 120 \text{ km}^3$ ($23 \pm 16\%$) of air from the top
301 10 m of firn. The corresponding decrease in FAC_{tot} indicates that, ~~as an upper estimate, potentially up to~~ $700 \pm 490 \text{ km}^3$ of air
302 may have been lost from the total firn column. In this we assume that the FAC₁₀ decrease propagated to the entire firn
303 column (see Section 2.5), which might not be accurate. Insufficient data are available to determine precisely how much FAC
304 was lost below 10 m and we can only give a hypothetical upper bound to the FAC_{tot} decrease.

305

306 Recent studies have identified increasing surface melt and meltwater refreezing as major contributors to increasing near-
307 surface firn densities, and subsequent loss of FAC (de la Peña et al., 2015; Charalampidis et al., 2015; Machguth et al., 2016;
308 Graeter et al., 2018). However, firn density and FAC are also dependent on annual snowfall, with decreasing snowfall
309 driving increasing firn density and decreasing FAC (e.g. Vandecrux et al., 2018). Nevertheless, the lack of widely distributed
310 observation of snow accumulation for the 1998-2017 period and the contradicting trends in precipitation calculated by RCMs
311 (Lucas-Picher et al., 2012; van den Broeke et al., 2016; Fettweis et al., 2017) complicate the partitioning of the melt and
312 snowfall contributions to changes in GrIS FAC-at-ice sheet scale.

313

314 To investigate how uncertainties in \overline{T}_a and \bar{c} impact our FAC₁₀ maps, we repeat our procedure using the 1979-2014 \overline{T}_a and \bar{c}
315 estimated by Box (2013) and Box et al. (2013) (hereafter referred to as “Box13”). The Box13-derived FAC₁₀ fits equally
316 well (RMSD < 0.3 m) to the FAC₁₀ observations, leading to spatially integrated FAC values within uncertainty of the MAR-
317 derived values. However, due to differing model formulations and atmospheric forcings, the spatial patterns of air
318 temperature and snowfall are different between Box13 and MARv3.5.2 (detailed in Fettweis et al. 2017), especially in the
319 southern and eastern regions of the firn area. This leads to different estimations of FAC₁₀ in these regions (Figure S4).
320 Additionally, in these regions no firn observations are available to constrain our FAC₁₀ estimates. More observations in the
321 sparsely observed southern and eastern regions would improve FAC₁₀ estimates and help better elucidate which \overline{T}_a and \bar{c}
322 source best describes the spatial pattern in FAC₁₀.

323 3.2. Firn retention capacity

324 The decrease in FAC_{10} in the LAPA between 1998-2008 and 2010-2017 translates to a loss in meltwater retention capacity
325 of 150 ± 100 Gt in the top 10 m of firn (Table 3). This ~~is equivalent to a potential sea level drawdown of~~ ~~lost retention~~
326 ~~capacity represents~~ 0.4 ± 0.3 mm sea level equivalent (s.l.e.). For the total firn column, we estimate an associated upper
327 bound loss of 540 ± 450 Gt (1.5 ± 1.2 mm s.l.e.). While these volumes are small compared to the average GrIS mass loss ~~of~~
328 ~~the ice sheet~~ ($171 \sim 0.47 \pm 1570.23$ Gtmm s.l.e. yr^{-1} for 1991–2015 in van den Broeke, 2016), the impact of reduced retention
329 capacity has an important time-integrated effect, in amplifying meltwater runoff each year. This amplification can be non-
330 linear as when, for instance, a succession anomalously high melt years and reduced firn permeability resulted in an abrupt
331 increase in western Greenland runoff in 2012 (Machguth et al. 2016).

332

333 Harper et al. (2012), using observations from 2007-2009, estimated that $150\,000$ km² of firn residing within the lower
334 percolation area (as delineated in an earlier version of MAR) could potentially store between 322 ± 44 Gt of meltwater in the
335 top 10 m of firn and $1\,289 \pm_{252}^{388}$ Gt within the entire firn column. We note that the Harper et al. (2012) estimate is based
336 solely on observations in the LAPA, while 68% of the percolation area to which they extrapolate is located in the HAPA. By
337 contrast, we find that the warmest $150\,000$ km² of our firn area in 2010-2017 can retain only 150 ± 66 Gt of meltwater in the
338 top 10 m of the firn. We estimate a total storage capacity of 310 ± 270 Gt within the whole firn column in this part of the firn
339 area. Our relatively low estimate of the retention capacity might reflect the recent decrease of FAC in the LAPA but also, for
340 the values derived from FAC_{tot} , our simplifying assumption that this decrease has propagated through the whole firn column
341 (Section 2.5). Yet, beyond these integrated values, our approach allows to quantify the firn retention capacity and the
342 corresponding uncertainty at any location of the firn area. Our product can therefore be used in combination with, for
343 instance, remotely sensed melt extent to derive which areas of the firn actively retain meltwater and evaluate the retention
344 capacity there.

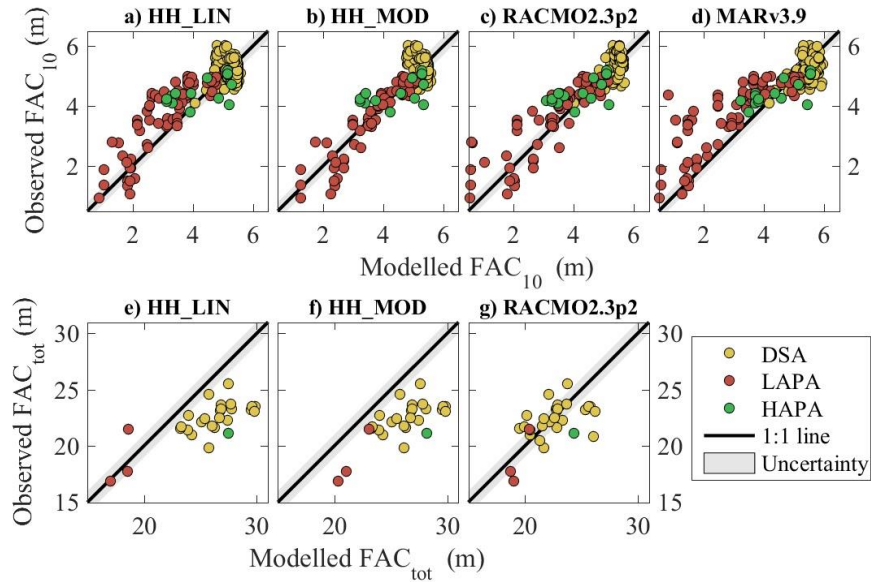
345

346 We use the same infiltration ice density as Harper et al. (2012), 843 ± 36 kg m⁻³ as determined from firn core segments
347 saturated by refrozen meltwater. However, Machguth et al. (2016) measured with similar technique an infiltration ice density
348 of 873 ± 25 kg m⁻³ in western Greenland. Using the latter value increases our estimated firn storage capacity of the top 10 m
349 of firn by 8 to 13%, depending on the region, but remains within our uncertainty intervals (Table 3). Additional field
350 measurements are needed to ascertain the spatial and temporal dependence of infiltration ice density on climatic drivers. Our
351 definition of retention capacity assumes that retention occurs through the refreezing of meltwater and neglects potential
352 liquid water retention seen in firn aquifers (Forster et al. 2014). Nevertheless, recent work in southeast Greenland showed
353 that meltwater resides less than 30 years in the aquifer before it flows into nearby crevasses and eventually leaves the ~~ice~~
354 ~~sheet~~GrIS (Miller et al. 2018). Meltwater refrozen within the firn can be retained for much longer periods, until it is

355 discharged at a marine-terminating outlet glacier or reaches the surface of the ablation area. By neglecting liquid water
 356 retention in firm, our study focuses on long-term meltwater retention.

357 3.3. Regional Climate Model evaluation

358 3.3.1. Comparison with FAC observations



359
 360 **Figure 6. Comparison between the observed FAC_{10} and FAC_{tot} and the simulated FAC in the corresponding cells of three RCMs.**

361 All models reproduce the FAC_{10} observations in the DSA and HAPA with bias ≤ 0.2 m and RMSD ≤ 0.4 m (Figure 6, Table
 362 5). RACMO2.3p2, MARv3.9, and HH_LIN tend to underestimate the FAC_{10} in the LAPA, while HH_MOD does not show a
 363 pronounced bias there. The RCMs all present a RMSD less than 12% of the mean FAC_{10} for our entire dataset. The RCMs
 364 are also evaluated against the 29 directly observed FAC_{tot} (Figure 6, Table 5). Both versions of HIRHAM5 overestimate
 365 FAC_{tot} in the DSA (bias > 3 m), while RACMO2.3p2 performs better in that area (bias = 0.1, RMSD = 1.8). HH_LIN and
 366 RACMO2.3p2 compare relatively well with the three FAC_{tot} observations available in the LAPA, while HH_MOD presents
 367 a larger positive bias. These three FAC_{tot} observations are located in the upper LAPA and therefore not including regions
 368 where RCMs underestimate FAC_{10} . All models overestimate the only FAC_{tot} observation available in the HAPA by more
 369 than 3 m. Compared to all FAC_{tot} measurements, RACMO2.3p2 gives a RMSD equivalent to 9% of the mean observed
 370 FAC_{tot} when HIRHAM5's RMSD reaches 20% with HH_MOD. None of the RCMs therefore simulate both FAC_{10} and
 371 FAC_{tot} accurately.

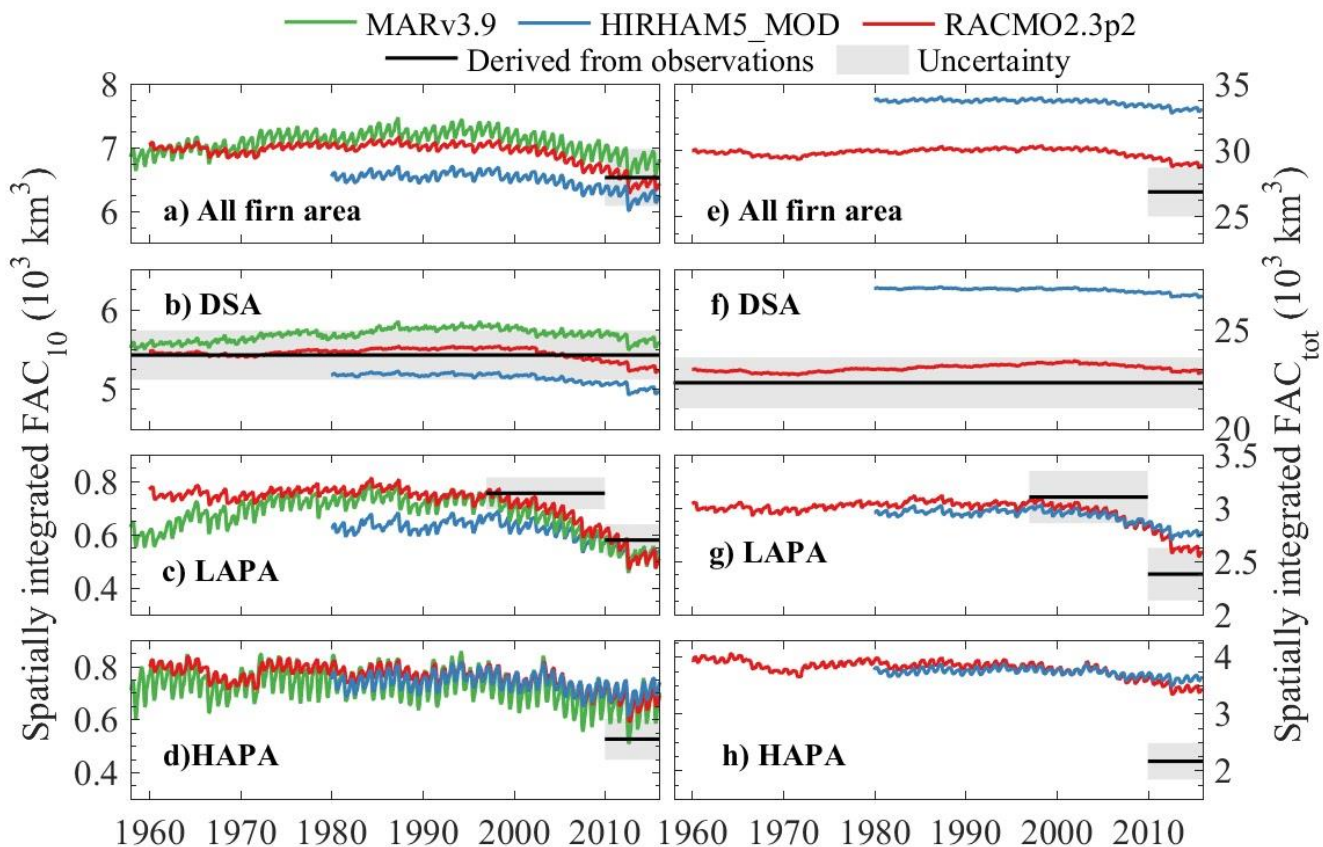
372

373 **Table 5. Performance of the RCMs for FAC_{10} and FAC_{tot} in terms of bias (average difference between model and observations)
 374 and Root Mean Squared Difference (RMSD).**

		DSA		LAPA		HAPA		All firm area	
		Bias (m)	RMSD (m)	Bias (m)	RMSD (m)	Bias (m)	RMSD (m)	Bias (m)	RMSD (m)
N _{obs}		259		82		19		360	
FAC ₁₀	HH_LIN	0.0	0.4	-0.5	0.8	0.1	0.6	-0.2	0.6
	HH_MOD	0.0	0.4	0.1	0.4	0.2	0.6	0.0	0.4
	RACMO2.3p2	0.1	0.3	-0.3	0.6	0.0	0.5	0.0	0.5
	MARv3.9	0.2	0.3	-0.6	1.0	0.2	0.6	0.0	0.6
N _{obs}		25		3		1		29	
FAC _{tot}	HH_LIN	3.7	4.1	1.0	3.3	6.4	-	3.4	4.1
	HH_MOD	3.8	4.1	3.7	4.1	7.1	-	3.9	4.3
	RACMO2.3p2	0.1	1.8	1.0	1.6	3.3	-	0.4	1.9

3.3.2. Comparison with the spatially integrated FAC

Agreement between RCM-simulated and observation-derived spatially integrated FAC is model- and region-dependent (Figure 7). RCMs simulate a spatially integrated FAC₁₀ within the uncertainty of our observation-derived estimation in the DSA. Models also show lower spatially integrated FAC₁₀ in the LAPA and higher values in the HAPA compared to our estimate (Figure 7b-d). These regional differences cancel out when spatially integrating FAC₁₀ over the entire firm area (Figure 7a). Our estimation of spatially integrated FAC_{tot} is subject to more assumptions as uncertainty is introduced in our conversion of FAC₁₀ to FAC_{tot} (Section 2.5). In the DSA, HH_MOD simulates a spatially integrated FAC_{tot} 20% higher than our estimation while RACMO2.3p2 simulates spatially integrated FAC_{tot} within our uncertainty range (Figure 7e). In the LAPA, the decrease in spatially integrated FAC_{tot} is more pronounced in our estimate than in the RCMs. This might indicate that, in the RCMs, the FAC loss is concentrated in the near-surface firm and has not yet propagated through the entire firm column. Our estimate assumes that any change in FAC₁₀ immediately propagates to the entire firm pack (see Section 2.5). In the HAPA, RCMs show higher spatially integrated FAC_{tot} values than our estimate (Figure 7h), contributing to the higher spatially integrated FAC_{tot} across the entire firm area in the RCMs compared to our estimation (Figure 7e). This is partly due to the fact that in our estimation, FAC decrease with elevation and is set to zero at the firm line. In the RCMs, modelled FAC remains higher than our estimate in the lower HAPA and in the vicinity of the firm line. No FAC observations are available in the lower HAPA to confirm this. Future measurements will help to quantify FAC in the surrounding of the firm line, allowing to better evaluate our assumptions and further assess the RCMs' performance in that area.



394

395 **Figure 7. Spatially integrated FAC in the RCMs and from observation-derived estimates.**

396 The differences between RCM outputs may stem from their respective surface forcings. As an illustration, HH_MOD uses a
 397 higher albedo than HH_LIN, thus calculates less surface melt and refreezing and, as a consequence, higher FAC_{10} in the
 398 LAPA. Noël et al. (2018) found that the surface mass balance of RACMO2.3p2 in the accumulation area was on average
 399 slightly lower than observations, indicating excessive sublimation or runoff relative to snowfall in the model. This surface
 400 bias could explain the model's underestimation of FAC_{10} in the LAPA at point scale (Figure 6, Table 5) and on spatially
 401 integrated values (Figure 7). On the other hand, MARv3.9 has slight positive biases in surface mass balance compared to
 402 observations (Fettweis et al. 2017). And although this RCM simulates too much precipitation relative to melt, it also
 403 underestimates FAC_{10} in the LAPA. Surface forcing is therefore not the only factor influencing the FAC estimates by the
 404 RCMs.

405

406 Differences in RCM-simulated FAC_{10} can also be explained by the way firn densification is treated in the snow model of
 407 each RCM. For instance, the overestimation of FAC_{tot} in the DSA by HIRHAM5 potentially arises from the use of a firn
 408 compaction law originally developed for seasonal snow (Vionnet et al., 2012). RACMO2.3p2 produces more realistic FAC_{tot}
 409 in the DSA, most likely because the densification law it uses has been tuned to match 8 deep firn density observations

410 (Kuipers Munneke et al., 2015a). It is nevertheless difficult to disentangle the roles of surface forcing and model formulation
411 in the performance of RCMs.

412

413 In agreement with our observation-derived FAC_{10} estimates, the RCMs calculate a decreasing FAC_{10} in the LAPA (Figure
414 7c) initiating in the early 2000s and accelerated during the extreme summers of 2010 and 2012. In the DSA, RCMs show a
415 FAC_{10} decrease ranging from -120 km^3 in MARv3.9 to -282 km^3 in RACMO2.3p2 between 1998 and 2017. These decreases
416 contradict with our conclusion that FAC has not changed significantly in the DSA over that period (Section 3.1). The
417 different FAC_{10} dynamics in our dataset and in RCMs could be due to: i) the RCMs not capturing an increase of snowfall in
418 the DSA which could in theory counterbalance the densification expected from the recent warming in the firn area (McGrath
419 et al., 2014); ii) an overestimated response of firn compaction rates to increasing temperatures in the models; iii) the spatial
420 heterogeneity and uncertainty of FAC observations leading to spurious conclusions from our dataset. Yet, finding identical
421 firn density profiles decades apart at several sites (e.g. Summit, Camp Century) adds confidence to our findings.

422 4. Conclusions

423 Using a collection of 360 firn density profiles spanning 65 years we quantified the firn air content (FAC) on the Greenland
424 ice sheet as function of long-term air temperature and net snow accumulation averages ($\overline{T_a}$ and \bar{c}). For the 2010-2017 period
425 we calculate that the Greenland firn contained $26\,800 \pm 1\,840 \text{ km}^3$ of air, of which $6\,500 \pm 450 \text{ km}^3$ in its top 10 m. We find
426 that over the 1953-2017 period, FAC remained constant within uncertainty in the dry snow area (DSA, where $\overline{T_a} \leq -19^\circ\text{C}$).
427 We note that the vast majority of the ice sheet's FAC ($83 \pm 5 \%$) resides within the DSA, and represents a potential
428 meltwater storage volume of $12\,800 \pm 1\,170 \text{ Gt}$. In the low accumulation percolation area (LAPA, where $\overline{T_a} > -19^\circ\text{C}$ and $\bar{c} \leq$
429 $600 \text{ mm w.eq. yr}^{-1}$), we calculate that the FAC decreased by $23 \pm 16\%$ between 1998-2008 and 2010-2017. This decrease
430 translates into the loss of meltwater retention capacity of $150 \pm 100 \text{ Gt}$ ($0.4 \pm 0.3 \text{ mm}$ sea level equivalent) in the top 10 m of
431 the firn and potentially up to $540 \pm 4450 \text{ Gt}$ ($1.5 \pm 1.2 \text{ mm}$ sea level equivalent) in the entire vertical extent of the firn layer.
432 This decreased FAC and meltwater retention capacity is focused in the lower accumulation area of central western
433 Greenland. Thus, in contrast to the relative stability of the DSA, the LAPA is the focal area of the firn's response to recent
434 climate change. The firn in the high accumulation percolation area (LAPA, where $\overline{T_a} > -19^\circ\text{C}$ and $\bar{c} > 600 \text{ mm w.eq. yr}^{-1}$)
435 has the capacity to store $370 \pm 70 \text{ Gt}$ in its top 10 m and up to $960 \pm 290 \text{ Gt}$ in its entire vertical extent. Yet, this area is
436 covered by fewer observations and would highly benefit from future field surveys.

437 The outputs from three regional climate models (HIRHAM5, RACMO2.3p2 and MARv3.9) indicate that our calculated
438 decrease in FAC may have been initiated in the early 2000's and accelerated after 2010. The RCMs also provide estimates of
439 FAC in regions where no measurements are available. But the mismatch between RCMs and our firn core dataset illustrates
440 that RCMs should be used with caution when assessing meltwater retention capacity, or when converting ice sheet volume

441 changes into mass changes in the firn area. Finally, our study highlights the importance of assimilating in situ firn density
442 measurements to document the climate response of ice-sheet firn as a non-trivial component of the sea-level budget. More
443 broadly, this work illustrates how new insight can be ~~gleaned-obtained~~ from the synthesis of historical data sources, and thus
444 emphasizes the tremendous value of open-access data within the scientific community.

445 5. Acknowledgement

446 This work is part of the Retain project funded by ~~Danmarks Frie Forskningsfond the Danish Council for Independent~~
447 ~~research~~ (Grant no. 4002-00234) and the Programme for Monitoring of the Greenland Ice Sheet (www.PROMICE.dk). The
448 field campaigns were funded by the NASA grant NNX15AC62G in collaboration with the Greenland Analogue Project
449 (GAP). Achim Heilig was supported by DFG grant HE 7501/1-1. We thank Hubertus Fischer from the Department of
450 Climate and Environmental Physics at University of Bern (Switzerland), for providing low resolution density data from firn
451 cores collected during the EGIG expeditions 1990 and 1992. We are grateful to Peter Langen from the Danish
452 Meteorological Institute, Stefan Ligtenberg from the Institute for Marine and Atmospheric Research at Utrecht University
453 (IMAU) and Xavier Fettweis from the Laboratory of Climatology, Department of Geography, University of Liège,
454 ~~(Belgium)~~ for providing the regional climate model output. We thank Sergey Marchenko and an anonymous reviewer for
455 their suggestions, which greatly improved the manuscript.

456 6. Data Availability

457 The FAC dataset, maps along with the firn area delineation are available at <https://arcticdata.io/>
458 <http://doi.org/10.18739/A2V40JZ6C> and the majority of the original firn density measurements can be found in the SUMup
459 dataset at <https://doi.org/10.18739/A2JH3D23R>. The source code is available at
460 github.com/BaptisteVandecrux/FAC10_study.

461 7. References

- 462 Albert, M., and Shultz, E.: Snow and firn properties and air–snow transport processes at Summit, Greenland, Atmos.
463 Environ., 36, 2789-2797, [https://doi.org/10.1016/S1352-2310\(02\)00119-X](https://doi.org/10.1016/S1352-2310(02)00119-X), 2002.
- 464 Alley, R.: Transformations in Polar Firn, Ph.D. Thesis, University of Wisconsin, Madison, WI, USA, 1987.

- 465 Bader, H.: Sorge's law of densification of snow on high polar glaciers, *J. of Glaciol.* , 2, 15, 319-411,
466 <https://doi.org/10.3189/S0022143000025144>, 1954.
- 467 Baker, I.: Density and permeability measurements with depth for the NEEM 2009S2 firn core, ACADIS Gateway,
468 <https://doi.org/10.18739/A2Q88G>, 2012.
- 469 Benson, C. S.: Stratigraphic Studies in the Snow and Firn of the Greenland Ice Sheet, U.S. Army Snow, Ice and Permafrost
470 Research Establishment, 1962.
- 471 Bindoff, N.L., P.A. Stott, K.M. AchutaRao, M.R. Allen, N. Gillett, D. Gutzler, K. Hansingo, G. Hegerl, Y. Hu, S. Jain, I.I.
472 Mokhov, J. Overland, J. Perlwitz, R. Sebbari and X. Zhang: Detection and Attribution of Climate Change: from
473 Global to Regional, in: *Climate Change 2013: The Physical Science Basis. Contribution of Working Group I to the*
474 *Fifth Assessment Report of the Intergovernmental Panel on Climate Change*, edited by: Stocker, T.F., D. Qin, G.-K.
475 Plattner, M. Tignor, S.K. Allen, J. Boschung, A. Nauels, Y. Xia, V. Bex and P.M. Midgley, Cambridge University
476 Press, Cambridge, United Kingdom and New York, NY, USA, pp. 867–952,
477 <https://doi.org/10.1017/CBO9781107415324.022>, 2013.
- 478 Bolzan, J. F., and Strobel, M.: Oxygen isotope data from snowpit at GISP2 Site 15., PANGAEA,
479 <https://doi.org/10.1594/PANGAEA.55511>, 1999.
- 480 Box, J.: Greenland ice sheet mass balance reconstruction. Part II: Surface mass balance (1840-2010), *J. Climate*, 26, 6974-
481 6989, <https://doi.org/10.1175/JCLI-D-12-00518.1>, 2013.
- 482 Box, J., Cressie, N., Bromwich, D. H., Jung, J.-H., van den Broeke, M. R., van Angelen, J., Forster, R.R., Miège, C., Mosley-
483 Thompson, E., Vinther, B., McConnell, J. R.: Greenland ice sheet mass balance reconstruction. Part I: Net snow
484 accumulation (1600-2009), *J. Climate*, 26, 3919-3934, <https://doi.org/10.1175/JCLI-D-12-00373.1>, 2013.

- 485 Braithwaite, R., Laternser, M., and Pfeffer, W. T.: Variation of near-surface firn density in the lower accumulation area of
486 the Greenland ice sheet, Pâkitsoq, West Greenland, *J. Glaciol.*, 40, 136, 477-485,
487 <https://doi.org/10.3189/S002214300001234X>, 1994.
- 488 Buchardt, S. L., Clausen, H. B., Vinther, B. M., and Dahl-Jensen, D.: Investigating the past and recent delta 18O-
489 accumulation relationship seen in Greenland ice cores, *Clim. Past*, 8, 6, 2053-2059, [https://doi.org/10.5194/cp-8-
490 2053-2012](https://doi.org/10.5194/cp-8-2053-2012), 2012.
- 491 Charalampidis, C., Van As, D., Box, J. E., van den Broeke, M. R., Colgan, W. T., Doyle, S. H., Hubbard, A. L., MacFerrin,
492 M., Machguth, H. and Smeets, C. J.: Changing surface-atmosphere energy exchange and refreezing capacity of the
493 lower accumulation area, West Greenland, *Cryosphere*, 9, 6, 2163-2181, <https://doi.org/10.5194/tc-9-2163-2015>,
494 2015.
- 495 Clausen, H., Gundestrup, N. S., Johnsen, S. J., Binchadler, R., and Zwally, J.: Glaciological investigations in the Crete area,
496 Central Greenland: a search for a new deep-drilling Site, *Ann. Glaciol.*, 10, 10-15,
497 <https://doi.org/10.3189/S0260305500004080>, 1988.
- 498 Colgan, W., Pedersen, A., Binder, D., Machguth, H., Abermann, J., and Jayred, M.: Initial field activities of the Camp
499 Century Climate Monitoring Programme in Greenland. *Geol. Surv. Denmark Greenland Bull.*, 41, 75-78, [pdf](#), 2018.
- 500 de la Peña, S., Howat, I. M., Nienow, P. W., van den Broeke, M. R., Mosley-Thompson, E., Price, S. F., Mair, D., Noël, B.,
501 and Sole, A. J.: Changes in the firn structure of the western Greenland Ice Sheet caused by recent warming,
502 *Cryosphere*, 9, 1203-1211, <https://doi.org/10.5194/tc-9-1203-2015>, 2015.
- 503 Fausto, R., Mayer, C., Ahlstrøm, A.: Satellite-derived surface type and melt area of the Greenland ice sheet using MODIS
504 data from 2000 to 2005, *Ann. Glaciol.*, 46, 35-42. <https://doi.org/10.3189/172756407782871422>, 2007.
- 505 Fausto, R. S., Andersen, S. B., Ahlstrøm, A. P., van As, D., Box, J. E., Binder, D., Citterio, M., Colgan, W., Haubner, K.,
506 Hansen, K., Karlsson, N. B., Mankoff, K. D., Pedersen, A. Ø., Solgaard, A. and Vandecrux, B.: The Greenland ice

507 sheet – snowline elevations at the end of the melt seasons from 2000 to 2017, Geol. Surv. Denmark Greenland
508 Bull., 41, 71-74, [pdf](#), 2018a.

509 Fausto, R. S., Box, J. E., Vandecrux, B., van As, D., Steffen, K., MacFerrin, M., Machguth H., Colgan W., Koenig L. S.,
510 McGrath D., Charalampidis C. and Braithwaite, R. J.: A Snow Density Dataset for Improving Surface Boundary
511 Conditions in Greenland Ice Sheet Firn Modeling, Front. Earth Sci., 6, 51, <https://doi.org/10.3389/feart.2018.00051>,
512 2018b.

513 Fettweis, X., Box, J. E., Agosta, C., Amory, C., Kittel, C., Lang, C., van As, D., Machguth, H., and Gallée, H.:
514 Reconstructions of the 1900–2015 Greenland ice sheet surface mass balance using the regional climate MAR
515 model, Cryosphere, 11, 2, 1015-1033, <https://doi.org/10.5194/tc-11-1015-2017>, 2017.

516 Fischer, H., Wagenbach, D., Laternser, M., and Haeberli, W.: Glacio-meteorological and isotopic studies along the EGIG
517 line, central Greenland., J. of Glaciol., 41, 139, 515-527, <https://doi.org/10.3189/S0022143000034857>, 1995.

518 Forster, R. R., Box, J. E., van den Broeke, M. R., Miège, C., Burgess, E. W., Angelen, J. H., Lenaerts, J. T. M., Koenig, L.
519 S., Paden, J., Lewis, C., Gogineni, S. P., Leuschen, C., and McConnell, J. R.: Extensive liquid meltwater storage in
520 firn within the Greenland ice sheet., Nat. Geosci., 7, 95-19, <https://doi.org/10.1038/NGEO2043>, 2014.

521 Graeter, K. A., Osterberg, E., Ferris, D. G., Hawley, R. L., Marshall, H. P., Lewis, G., Meehan, T., McCarthy, F., Overly, T.
522 and Birkel, S.D., and Birkel, S.: Ice Core Records of West Greenland Melt and Climate Forcing, Geophys. Res.
523 Lett., 45, 7, <https://doi.org/10.1002/2017GL076641>, 2018.

524 Harper, J., Humphrey, N., Pfeffer, W. T., Brown, J., and Fettweis, X.: Greenland ice-sheet contribution to sea-level rise
525 buffered by meltwater storage in firn, Nature, 491, 240-243, <https://doi.org/10.1038/nature11566>, 2012.

526 Hawley, R. L., Courville, Z. R., Kehrl, L., Lutz, E., Osterberg, E., Overly, T. B., and Wong, G.: Recent accumulation
527 variability in northwest Greenland from ground-penetrating radar and shallow cores along the Greenland Inland
528 Traverse, J. Glaciol., 60, 220, 375-382, <https://doi.org/10.3189/2014JoG13J141>, 2014.

- 529 Heilig, A., Eisen, O., MacFerrin, M., Tedesco, M., and Fettweis, X.: Seasonal monitoring of melt and accumulation within
530 the deep percolation zone of the Greenland Ice Sheet and comparison with simulations of regional climate
531 modeling, *Cryosphere*, 12, 1851-1866, <https://doi.org/10.5194/tc-12-1851-2018>, 2018.
- 532 Humphrey, N. F., Harper, J. T., and Pfeffer, W. T.: Thermal tracking of meltwater retention in Greenland's accumulation
533 area, *J. Geophys. Res.*, 117, F01010, <https://doi.org/10.1029/2011JF002083>, 2012.
- 534 Jezek, K. C.: Surface Elevation and Velocity Changes on the South Central Greenland Ice Sheet: 1980-2011 - Data
535 Summary. BPRC Technical Report No. 2012-01, Byrd Polar Research Center, The Ohio State University,
536 Columbus, Ohio, 2012.
- 537 Kameda, T., Narita, H., Shoji, H., Nishio, F., Fuji, Y., and Watanabe, O.: Melt features in ice cores from Site J, southern
538 Greenland: some implication for summer climate since AD 1550, *Ann. Glaciol.*, 21, 51-58,
539 <https://doi.org/10.3189/S0260305500015597>, 1995.
- 540 Koenig, L. S., Miège, C., Forster, R. R., and Brucker, L.: Initial in situ measurements of perennial meltwater storage in the
541 Greenland firn aquifer, *Geophys. Res. Lett.*, 41, 81-85, <https://doi.org/10.1002/2013GL058083>, 2014.
- 542 Kovacs, A., Weeks, W. F., and Michitti, F.: Variation of Some Mechanical Properties of Polar Snow, Camp Century,
543 Greenland, CRREL Res. Rpt. 276, 1969.
- 544 Kuipers Munneke, P., Ligtenberg, S. R. M., Noël, B. P. Y., Howat, I. M., Box, J. E., Mosley-Thompson, E., McConnell, J.
545 R., Steffen, K., Harper, J. T., Das, S. B., and van den Broeke, M. R.: Elevation change of the Greenland Ice Sheet
546 due to surface mass balance and firn processes, 1960–2014, *Cryosphere*, 9, 2009–2025, [https://doi.org/10.5194/tc-9-
547 2009-2015](https://doi.org/10.5194/tc-9-2009-2015), 2015a.
- 548 Kuipers Munneke, P., Ligtenberg, S.R., Suder, E.A. and van den Broeke, M.R.: A model study of the response of dry and
549 wet firn to climate change. *Ann. Glaciol.*, 56(70), pp.1-8, <https://doi.org/10.3189/2015AoG70A994>, 2015b.

- 550 Langen, P., Fausto, R. S., Vandecrux, B., Mottram, R., and Box, J.: Liquid Water Flow and Retention on the Greenland Ice
551 Sheet in the Regional Climate Model HIRHAM5: Local and Large-Scale Impacts., *Front. Earth Sci.*, 4, 110,
552 <https://doi.org/10.3389/feart.2016.00110>, 2017.
- 553 Langway, C. C.: Stratigraphic analysis of a deep ice core from Greenland, *CRREL Res. Rpt. 77*, 1967.
- 554 Ligtenberg, S. R., Kuipers Munneke, P., Noël, B. P., and . van den Broeke, M.: Improved simulation of the present-day
555 Greenland firn layer (1960–2016), *Cryosphere*, <https://doi.org/10.5194/tc-12-1643-2018>, 2018.
- 556 Lomonaco, R., Albert, M., and Baker, I.: Microstructural evolution of fine-grained layers through the firn column at Summit,
557 Greenland, *J. Glaciol.*, 57, 204, <https://doi.org/10.3189/002214311797409730>, 2011.
- 558 Lucas-Picher, P., Wulff-Nielsen, M., Christensen, J. H., Aðalgeirsdóttir, G., Mottram, R., and Simonsen, S.: Very high
559 resolution in regional climate model simulations for Greenland: Identifying added value, *J. Geophys. Res.*, 117,
560 D02108, <https://doi.org/10.1029/2011JD016267>, 2012.
- 561 Machguth, H., MacFerrin, M., As, D. v., Box, J., Charalampidis, C., Colgan, W., Fausto, R.S., Meijer, H.A., Mosley-
562 Thompson, E. and van de Wal, R.S.: Greenland meltwater storage in firn limited by near-surface ice formation,
563 *Nature Clim. Change*, 6, 390-395, <https://doi.org/10.1038/NCLIMATE2899>, 2016.
- 564 Mayewski, P., and Whitlow, S.: Snow Pit and Ice Core Data from Southern Greenland, 1984, NSF Arctic Data Center.
565 <https://doi.org/10.5065/D6S180MH>, 2016a.
- 566 Mayewski, P., and Whitlow S.: Snow Pit Data from Greenland Summit, 1989 to 1993. NSF Arctic Data Center.
567 <https://doi.org/10.5065/D6NP22KX>, 2016b.
- 568 McGrath, D., Colgan, W., Bayou, N., Muto, A. and Steffen, K.. Recent warming at Summit, Greenland: Global context and
569 implications. *Geophys. Res. Lett.* 40, 2091-2096, <https://doi.org/10.1002/grl.50456>, 2013.

- 570 Miège, C., Forster R.R., Box J.E., Burgess, E., McConnell, J., Pasteris, D., and Spikes, V. B.: Southeast Greenland high
571 accumulation rates derived from firn cores and ground-penetrating radar, *Ann. Glaciol.*, 54, 63, 322-332,
572 <https://doi.org/10.3189/2013AoG63A358>, 2013.
- 573 Miège, C., Forster, R.R., Brucker, L., Koenig, L.S., Solomon, D.K., Paden, J.D., Box, J.E., Burgess, E.W., Miller, J.Z.,
574 McNerney, L. and Brautigam, N.: Spatial extent and temporal variability of Greenland firn aquifers detected by
575 ground and airborne radars. *J. Geophys. Res.-Earth*, 121, 12, 2381-2398, <https://doi.org/10.1002/2016JF003869>,
576 2016.
- 577 Morris, E. M., and Wingham, D. J.: Densification of polar snow: Measurements, modeling and implication for altimetry, *J.*
578 *Geophys. Res.-Earth*, <https://doi.org/10.1002/2013JF002898>, 2014.
- 579 Mosley-Thompson, E., McConnell, J., Bales, R., Li, Z., Lin, P.-N., and Steffen, K.: Local to regional-scale variability of
580 annual net accumulation on the Greenland ice sheet from PARCA cores, *J. Geophys. Res.*, 106, 33839–33851,
581 <https://doi.org/10.1029/2001JD900067>, 2001.
- 582 Mote T. L.: Greenland surface melt trends 1973–2007: Evidence of a large increase in 2007, *Geophys. Res. Lett.*, 34(22),
583 <https://doi.org/10.1029/2007GL031976>, 2007.
- 584 Nerem R. S., Beckley B. D., Fasullo J. T., Hamlington B. D., Masters D, Mitchum G. T.: Climate-change–driven accelerated
585 sea-level rise detected in the altimeter era. *P. Natl. Acad. Sci. U.S.A.*, 7:201717312,
586 <https://doi.org/10.1073/pnas.1717312115>, 2018.
- 587 Nghiem, S.V., Hall, D.K., Mote, T.L., Tedesco, M., Albert, M.R., Keegan, K., Shuman, C.A., DiGirolamo, N.E. and
588 Neumann, G.: The extreme melt across the Greenland ice sheet in 2012, *Geophys. Res. Lett.*, 39, L20502,
589 <https://doi.org/10.1029/2012GL053611>, 2012.
- 590 Noël, B., van de Berg, W. J., van Wessem, J. M., van Meijgaard, E., van As, D., Lenaerts, J. T. M., Lhermitte, S., Kuipers
591 Munneke, P., Smeets, C. J. P. P., van Ulf, L. H., van de Wal, R. S. W., and van den Broeke, M. R.: Modelling the

592 climate and surface mass balance of polar ice sheets using RACMO2 – Part 1: Greenland (1958–2016), *The*
593 *Cryosphere*, 12, 811-831, <https://doi.org/10.5194/tc-12-811-2018>, 2018.

594 Porter, S., and Mosley-Thompson, E.: Exploring seasonal accumulation bias in a west central Greenland ice core with
595 observed and reanalyzed data, *J. Glaciol.*, 60, 224, 1065-1074, <https://doi.org/10.3189/2014JoG13J233>, 2014.

596 Reed, S.: Performance Study of the Dewline Ice Cap Stations, 1963, CRREL Special Report 72, 1966.

597 Renaud, A.: Etude physiques et chimiques sur la glace de l'inlandsis du Groenland , *Medd. Groenland*, 2, 177, 100-107,
598 1959.

599 Shumskii P.A.: Principles of structural glaciology: the petrography of fresh-water ice as a method of glaciological
600 investigation. Dover Publications Inc..1964.

601 Simonsen, S.B., Stenseng, L., Adalgeirsdóttir, G., Fausto, R.S., Hvidberg, C.S. and Lucas-Picher, P.: Assessing a
602 multilayered dynamic firn-compaction model for Greenland with ASIRAS radar measurements. *J. Glaciol.*,
603 59(215), pp.545-558, <https://doi.org/10.3189/2013JoG12J158>, 2013.

604 Spencer, M. K., Aller, R. B., and Creyts, T. T.: Preliminary firn-densification model with 38-site dataset, *J. Glaciol.*, 47, 159,
605 671-676, <https://doi.org/10.3189/172756501781831765>, 2001.

606 Steen-Larsen, H.C., Masson-Delmotte, V., Sjolte, J., Johnsen, S.J., Vinther, B.M., Bréon, F.M., Clausen, H.B., Dahl-Jensen,
607 D., Falourd, S., Fettweis, X. and Gallée, H.: Understanding the climatic signal in the water stable isotope records
608 from the NEEM cores, *J. Geophys. Res.*, 116, D06108, <https://doi.org/10.1029/2010JD014311>, 2011.

609 Sørensen, L. S., Simonsen, S.B., Nielsen, K., Lucas-Picher, P., Spada, G., Adalgeirsdóttir, G., Forsberg, R. and Hvidberg,
610 C.: Mass balance of the Greenland ice sheet (2003–2008) from ICESat data–the impact of interpolation, sampling
611 and firn density. *Cryosphere*, 5, pp.173-186, <https://doi.org/10.5194/tc-5-173-2011>, 2011.

612 Vallelonga, P., Christianson, K., Alley, R. B., Anandakrishnan, S., Christian, J. E. M., Dahl-Jensen, D., Gkinis, V., Holme,
613 C., Jacobel, R. W., Karlsson, N. B., Keisling, B. A., Kipfstuhl, S., Kjær, H. A., Kristensen, M. E. L., Muto, A.,
614 Peters, L. E., Popp, T., Riverman, K. L., Svensson, A. M., Tibuleac, C., Vinther, B. M., Weng, Y., and Winstrup,
615 M.: Initial results from geophysical surveys and shallow coring of the Northeast Greenland Ice Stream (NEGIS),
616 Cryosphere, 8, 1275-1287, <https://doi.org/10.5194/tc-8-1275-2014>, 2014.

617 van Angelen, J., Lenaerts, J. T., van den Broeke, M. R., Fettweis, X., and van Meijgaard, E.: Rapid loss of firn pore space
618 accelerates 21st century Greenland mass loss, Geophys. Res. Lett., 40, 2109-2113,
619 <https://doi.org/10.1002/grl.50490>, 2013.

620 Vandecrux, B., Fausto, R.S., Langen, P.L., Van As, D., MacFerrin, M., Colgan, W.T., Ingeman-Nielsen, T., Steffen, K.,
621 Jensen, N.S., Møller, M.T. and Box, J.E.: Drivers of Firn Density on the Greenland Ice Sheet Revealed by Weather
622 Station Observations and Modeling, J. Geophys. Res.-Earth, <https://doi.org/10.1029/2017JF004597>, 2018.

623 van den Broeke, M. R., Enderlin, E. M., Howat, I. M., Kuipers Munneke, P., Noël, B. P. Y., van de Berg, W. J., van
624 Meijgaard, E., and Wouters, B.: On the recent contribution of the Greenland ice sheet to sea level change,
625 Cryosphere, 10, 1933-1046, <https://doi.org/10.5194/tc-10-1933-2016>, 2016.

626 van der Veen, C. J., Mosley-Thompson, E., Jezek, K. C., Whillans, I. M., and Bolzan, J. F.: Accumulation rates in South and
627 Central Greenland, Polar Geography, 25, 2, 79-162, <https://doi.org/10.1080/10889370109377709>, 2001.

628 Wilhelms, F.: Measuring the Conductivity and Density of Ice Cores, Ber. Polarforsch., 191, 1996.

629
630
631
632
633
634